metals

Article

Effect of Ge Addition on Magnetic Properties and Crystallization Mechanism of FeSiBPNbCu Nanocrystalline Alloy with High Fe Content

Haijie Zhang [1,2,3], Fushan Bai [1,2,3], Yaqiang Dong [2,4,*], Lei Xie [1,3], Qiang Li [1,3,*], Aina He [2,4] and Jiawei Li [2,4]

1 School of Physics Science and Technology, Xinjiang University, Urumqi 830046, China; zhanghaijie@nimte.ac.cn (H.Z.); baifushan@nimte.ac.cn (F.B.); 15199062962@163.com (L.X.)
2 Zhejiang Province Key Laboratory of Magnetic Materials and Application Technology, CAS Key Laboratory of Magnetic Materials and Devices, Ningbo Institute of Materials Technology & Engineering, Chinese Academy of Sciences, Ningbo 315201, China; hean@nimte.ac.cn (A.H.); lijw@nimte.ac.cn (J.L.)
3 Xinjiang Key Laboratory of Solid State Physics and Devices, Xinjiang University, Urumqi 830046, China
4 University of Chinese Academy of Sciences, Beijing 100049, China
* Correspondence: dongyq@nimte.ac.cn (Y.D.); qli@xju.edu.cn (Q.L.)

Abstract: In this work, new Ge-containing Fe-based nanocrystalline alloys with the composition of $Fe_{80.2}Si_3B_{12\text{-}x}P_2Nb_2Cu_{0.8}Ge_x$ (x = 0, 1, 2 at.%) were developed, and the effects of Ge content on the magnetic and crystallization processes of the alloys were investigated. The addition of Ge extends the annealing window of the present Fe-based alloys, which reaches 173.6 K for the alloy of x = 2. The nanocrystalline alloy of x = 2, composed of dense and uniformly distributed α-Fe grains with an average grain size of 15.7 nm precipitated in the amorphous matrix, was obtained by conventional annealing treatment at a temperature of 843 K for 10 min, and this nanocrystalline alloy exhibited excellent magnetic properties with the H_c of 3 A/m and B_s of 1.65 T, which has great potential for industrial application. Non-isothermal crystallization kinetics studies show that the nucleation activation energy of the alloys gradually decreases with the increase in Ge content. The primary crystallization process is dominated by the direct growth of pre-existing nuclei in the as-spun alloy ribbons, and these pre-existing nuclei provide numerous heterogeneous nucleation sites to form dense and uniform α-Fe nanocrystals with a fine grain size, which leads to the excellent magnetic properties of the present Ge-containing Fe-based nanocrystalline alloys.

Keywords: Fe-based nanocrystalline alloys; magnetic property; pre-existing nuclei; crystallization kinetics

check for updates

Citation: Zhang, H.; Bai, F.; Dong, Y.; Xie, L.; Li, Q.; He, A.; Li, J. Effect of Ge Addition on Magnetic Properties and Crystallization Mechanism of FeSiBPNbCu Nanocrystalline Alloy with High Fe Content. *Metals* **2022**, *12*, 640. https://doi.org/10.3390/met12040640

Academic Editor: Alberto Moreira Jorge Junior

Received: 12 March 2022
Accepted: 5 April 2022
Published: 8 April 2022

Publisher's Note: MDPI stays neutral with regard to jurisdictional claims in published maps and institutional affiliations.

1. Introduction

Fe-based amorphous/nanocrystalline soft magnetic alloys are widely used in wireless charging, transformers, sensors, etc. The renewal and iteration of technology requires the development of devices in the direction of miniaturization and high efficiency [1], so the shortcomings in magnetic properties of the existing alloys must be solved to make the overall performance of the alloy more excellent. Since the first discovery of the FeSiBNbCu nanocrystalline alloys in 1988 [2], Fe-based nanocrystalline alloys have attracted widespread attention due to their excellent performance. The Finemet alloy is widely used due to its ultra-high magnetic permeability (μ), extremely low coercivity (H_c) and excellent frequency characteristics, but the relative low saturation flux density (B_s) struggles to fulfill the demand of high efficiency and the miniaturization of the device [3,4]. The improvement of the B_s requires the content of ferromagnetic elements in the alloy to be as high as possible. Among the ferromagnetic elements of Fe, Co and Ni, the Co and Ni elements will increase the cost and likely deteriorate the magnetic properties of the alloy [5–7]; thus, increasing the Fe content is the most economical and effective way to improve B_s. However, for alloy systems with a high Fe content, it is very difficult to balance the high B_s and sufficient amorphous forming ability (AFA) at the same time because too high an Fe content will usually cause the alloy's AFA to decrease [8–11]. So, it is desirable to design a reasonable alloy composition to ensure both good soft magnetic properties and sufficient AFA of the alloy to achieve industrial production [12–14].

Many studies have shown that adding a P element can not only increase the AFA of alloy, but also has the effect of promoting nucleation and refining the grain of alloys [8,15,16]. Compared with P-free Fe-based alloys, P-containing Fe-based alloys have a higher activation energy, which helps to form a uniform density microstructure, and thus they have an excellent performance [17–19]. Additionally, the research of V. Cremacshi et al. shows that the addition of Ge can optimize magnetic properties and avoid the decrease in B_s of Fe-based nanocrystalline alloys [20–23]. Based on the above consideration, in this work, new $Fe_{80.2}Si_3B_{12-x}P_2Nb_2Cu_{0.8}Ge_x$ (x = 0, 1, 2 at.%) alloys were designed by adding P and Ge to a FINEMET-like nanocrystalline alloys with a high Fe content, the corresponding nanocrystalline alloys were prepared by conventional heat treatment, and the effects of Ge content on the magnetic properties and crystallization process of the present nanocrystalline alloys were investigated. The problems of rapid grain coarsening and the sudden decrease in the magnetic properties of Fe-based nanocrystalline soft magnetic alloys with a high Fe content during the annealing process were successfully solved by optimizing the composition of the alloys and the heat treatment process; therefore, the prepared nanocrystalline alloys exhibit excellent soft magnetic properties, and thus can be applied and industrialized.

2. Materials and Methods

The master alloy ingots of $Fe_{80.2}Si_3B_{12-x}P_2Nb_2Cu_{0.8}Ge_x$ (x = 0, 1, 2 at.%) were prepared using induction-melting technology by smelting a mixture of high-purity raw materials of Fe (99.99%), Si (99.99 wt.%), B (99.95%), FeP (99.99%), Cu (99.99%) and Nb (99.99%) in high-purity argon atmosphere. The broken alloy ingots were made into alloy ribbons with a thickness of 22 μm and a width of 1.2 mm by using melt spinning technique. The thermal behavior of the samples was measured by a differential scanning calorimeter (DSC, 404C, Netzsch, Shanghai, China) under the conditions of pure argon gas flow and a constant heating rate. The structural features of the alloy ribbon samples were detected by an X-ray diffraction (XRD, D8 ADVANCE, Bruker, Billerica, MA, USA) with Cu-$K\alpha$ radiation and transmission electron microscopy (Tecnai F20, FEI, Hillsboro, OR, USA). Tubular annealing furnace was used to anneal the melt-spun ribbons in a vacuum atmosphere to produce nanocrystalline alloy ribbons. The coercivity (H_c) of the annealed alloy ribbons was measured by a DC-BH loop tracer (EXPH-100, Riken Deshi, Saitama, Japan) under a magnetic field of 800 A/m. The saturation magnetic flux density (B_s) was measured by a vibrating sample magnetometer (VSM, 7410, Lake Shore, Westerville, OH, USA) at room temperature with a maximum applied field of 800 kA/m.

3. Results and Discussion

The melt-spun alloy ribbons of $Fe_{80.2}Si_3B_{12-x}P_2Nb_2Cu_{0.8}Ge_x$ (x = 0, 1 and 2 at.%, denoted as Ge0, Ge1 and Ge2, respectively) have outstanding surface quality and bending ductility. Figure 1a shows the XRD patterns taken from the free surface of the as-spun Ge0, Ge1 and Ge2 alloy ribbons, in which there are only diffuse peaks at around 2θ = 45°, and no sharp diffraction peaks corresponding to crystalline phases, indicating the formation of a complete amorphous phase.

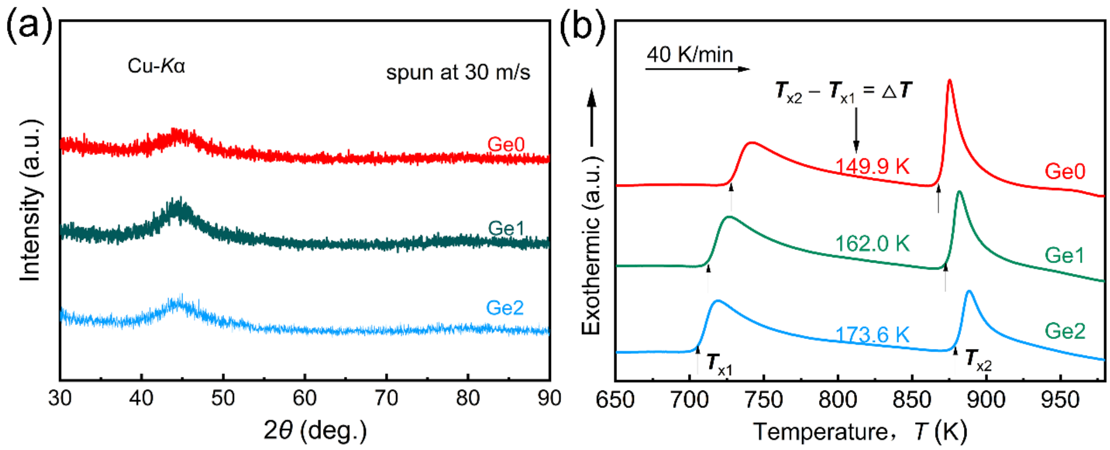

Figure 1. XRD patterns taken from the free surface (**a**) and DSC thermal scans (**b**) of the as-spun alloy ribbons.

Figure 1b shows DSC thermal curves of the as-spun Ge0, Ge1, and Ge2 alloy ribbons at a heating rate of 40 K/min. All of the DSC curves show two clear exothermic peaks. To determine the crystallization reaction corresponding to the two exothermic peaks, we continuously heated the Ge0, Ge1, and Ge2 glassy alloy ribbons to a temperature just beyond their T_{x1} (onset temperature of the first peak) and T_{x2} (onset temperature of the second peak), respectively, at a heating rate of 40 K/min, and then cooled down the glassy alloy ribbons to room temperature as fast as possible in a DSC. The XRD patterns of the produced samples are shown in Figure 2. It is indicated that the first and second exothermic peaks in the DSC curves correspond to the precipitation of the α-Fe phase and Fe_2(B,P) phases, respectively. Additionally, it can be seen that, as the Ge content increases, the T_{x1} and T_{x2} of the alloys shift toward the low- and high-temperature directions, respectively, causing ΔT (= $T_{x2} - T_{x1}$) to gradually increase from 149.9 K for the Ge0 to 173.6 K for the Ge2. A larger ΔT is better for promoting the precipitation of α-Fe and inhibiting the precipitation of borides and phosphides, which is more conducive to the preparation of dense and uniform nanocrystals.

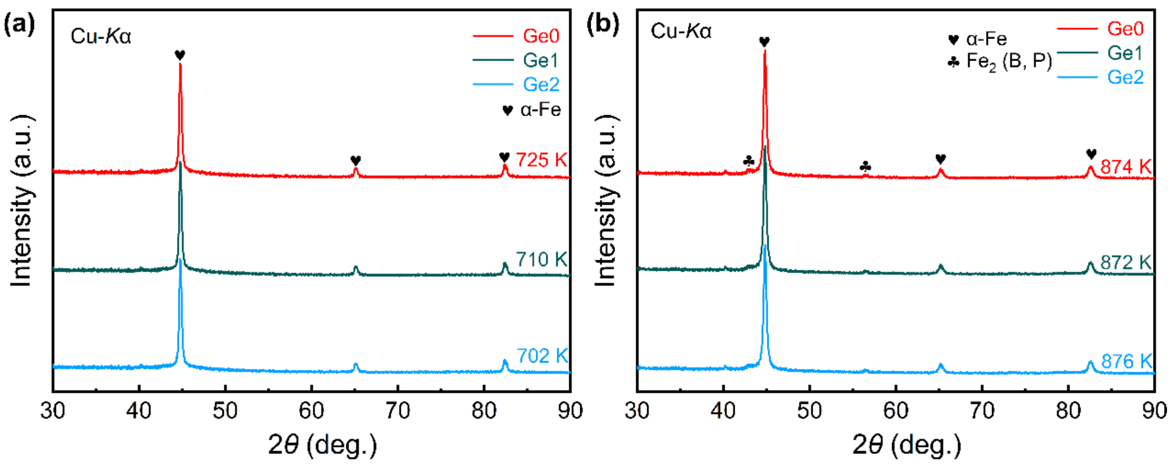

Figure 2. XRD patterns of $Fe_{80.2}Si_3B_{12\text{-}x}P_2Nb_2Cu_{0.8}Ge_x$ (x = 0, 1, 2 at.%) alloys produced by continuously heating to a temperature just beyond the T_{x1} (**a**) and T_{x2} (**b**) at a heating rate of 40 K/min and then cooling them down to room temperature as fast as possible in a DSC.

Heat treatment is one of the most commonly used methods to prepare nanocrystalline soft magnetic alloys from amorphous alloys. The Ge0, Ge1, and Ge2 melt-spun ribbons were subject to a conventional annealing treatment at different annealing temperature (T_A) for 10 min. Figure 3a shows the variation in H_c of the annealed alloy ribbons with the T_A.

It can be seen that, as the T_A rises from 743 K to 863 K, the H_c of the alloys first gradually decreases, reaches the lowest value at 843 K, and then rapidly increases. It is indicated that 843 K is the best annealing temperature for the nano-crystallization of the alloys, which may be due to the precipitation of a large number of dense and uniform nano-crystals by annealing at this temperature. By annealing below the optimal annealing temperature, only a small amount of crystal grains can be precipitated and properly coarsened, which causes an increase in the H_c of the alloys. By annealing above the optimal annealing temperature, hard magnetic phases, such as borides and phosphides, may be precipitated, which leads to a rapid increase in the H_c of the alloys. It can also be clearly seen from Figure 3a that the magnetic properties become better with the increase in the Ge content. This may be because the Ge is preferentially enriched in the remaining amorphous phase, which leads to an increase in the exchange stiffness of the intergranular region, reducing the magneto crystalline anisotropy effect of the alloy and making its soft magnetic properties more excellent.

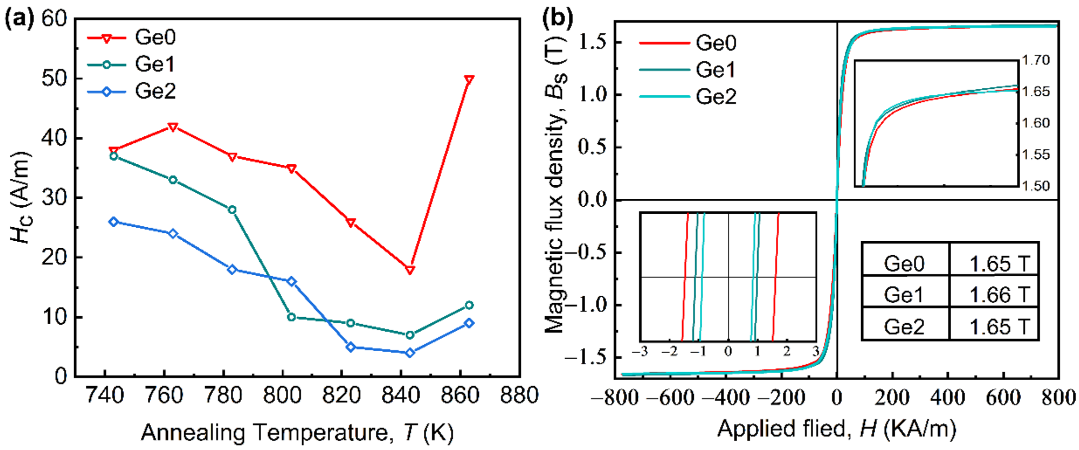

Figure 3. H_c of the $Fe_{80.2}Si_3B_{12\text{-}x}P_2Nb_2Cu_{0.8}Ge_x$ (x = 0, 1, 2 at.%) alloy ribbons annealed at different T_A by conventional annealing (**a**) and hysteresis loop and B_s of the alloys annealed by conventional annealing (843 K, 10 min) (**b**).

Figure 3b shows the B_s of the alloys annealed at 843 K for 10 min. It can be seen that the B_s of the annealed Ge0, Ge1, and Ge2 alloys is essentially the same. The saturation magnetic flux density of the Fe-based nanocrystalline alloy is the sum of the magnetic moments of the amorphous phase and the nanocrystalline phase. The relative Fe content of the Ge0, Ge1, and Ge2 alloys is very close, and thus their B_s has no significant difference. The partial enlargement in the inset of Figure 3b shows that the H_c of the nanocrystalline alloys gradually decreases with the increase in the Ge content. Among the three alloys annealed at 843 K for 10 min, the Ge2 alloy exhibits the best magnetic properties with the H_c of 3 A/m and the B_s of 1.65 T, which is enough to meet market requirements.

In order to explore the cause of the excellent soft magnetic properties of the Ge2 alloy annealed at 843 K for 10 min, the microscopic morphology of this alloy was observed by TEM, as shown in Figure 4. In Figure 4, it can be clearly seen that nano-scale grains with an average size of 15.7 nm are uniformly precipitated in the amorphous matrix; furthermore, these precipitated grains can be determined as the α-Fe phase through the identification of the selected area electron diffraction pattern. It is known that the H_c and grain size are positively correlated in nanocrystalline alloys. Therefore, the small, dense and uniform nanocrystalline structure of the annealed Ge2 alloy may account for its excellent magnetic properties.

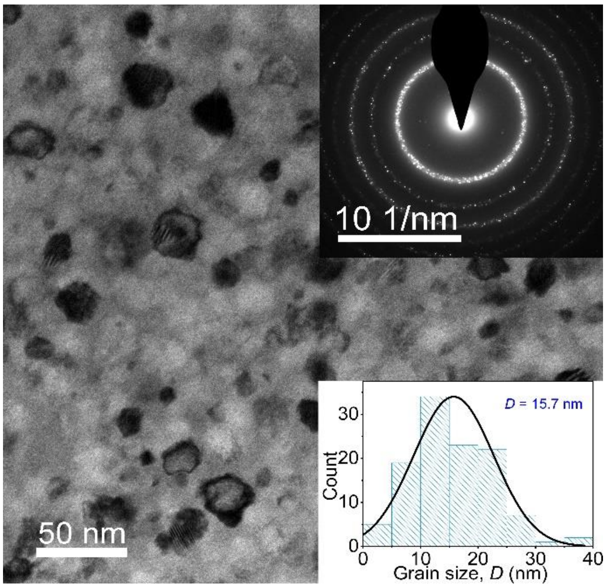

Figure 4. TEM bright field images with the corresponding selected area electron diffraction patterns and grain size distribution for the annealed Ge2 alloy ribbons.

The effective activation energy (E) of the alloys can be used to describe the difficulty of the crystallization process [24]. The effective activation energy can be determined by various methods [25–27]; here, it is calculated by the Kissinger equation as follows [26,27]:

$$\ln\left(\frac{T^2}{\beta}\right) = \frac{E}{RT} + constant, \quad (1)$$

where R is the ideal gas constant, T is the characteristic temperature at a certain heating rate β, and E is the effective activation energy of the transformation process related to the corresponding characteristic temperature. Based on Equation (1), a straight line, i.e., the Kissinger plot, can be obtained by drawing $\ln(T^2/\beta)$ against $1000/T$, and the slope of the straight line is equal to E/R and can be obtained by linear fitting, from which the effective activation energy E can be determined.

When the characteristic temperature T is taken as the onset crystallization temperature (T_x) and the crystallization peak temperature (T_p), respectively, the corresponding effective activation energy E is referred to as the nucleation activation energy (E_x) and the growth activation energy (E_p) of the crystallization reaction, respectively. The T_{x1} and T_p1 of the primary crystallization reaction can be determined from the DSC curves of the alloys, and the corresponding Kissinger plots for the two characteristic temperatures are shown in Figure 5. From the Kissinger plots, the E_x1 and E_p1 of the primary crystallization reaction can be calculated. The Curie temperature (T_c), T_{x1}, T_p1, E_x1 and E_p1 of the alloys are summarized in Table 1. It can be seen that both the E_x1 and E_p1 of the alloys gradually decrease with the increase in Ge content. In other words, the Ge2 alloy has the lowest nucleation and growth activation energies of the primary crystallization reaction among the three alloys. This is because the increase in the Ge content reduces the non-metallic element content in the alloys, which may lead to a decrease in the alloy's AFA. For alloys with a high Fe content, the reduction in AFA will result in a large number of pre-existing nuclei in the as-spun alloy ribbon, which will serve as heterogeneous nucleation sits to promote nucleation and thus reduce the nucleation activation energy. The decrease in the growth activation energy is because, as the crystallization progresses, the B and Nb elements insoluble in the α-Fe phase are continuously enriched in the alloy, which stabilizes the amorphous phase and makes the precipitation of the hard magnetic phase more difficult.

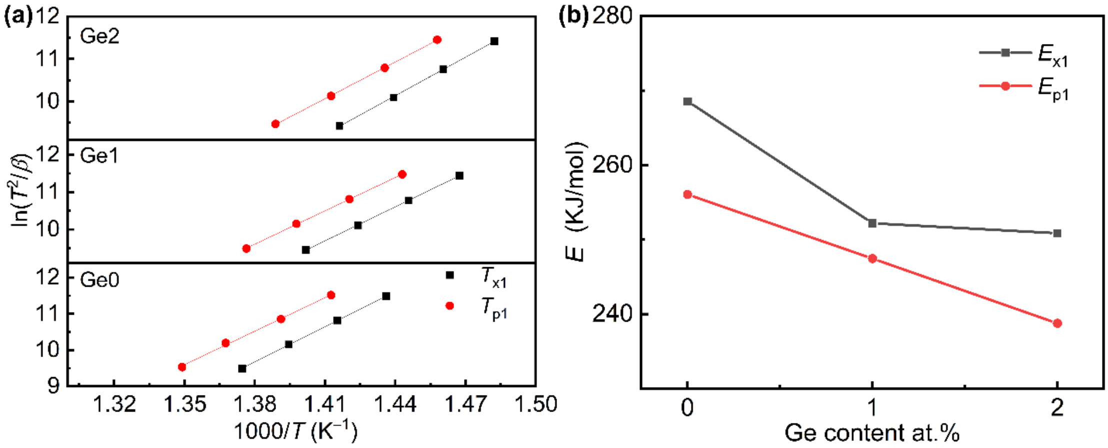

Figure 5. Kissinger plots for the T_{x1} and T_{p1} (**a**) and the changes in the activation energies determined from Kissinger plots with the alloy composition (**b**) of the as-spun $Fe_{80.2}Si_3B_{12\text{-}x}P_2Nb_2Cu_{0.8}Ge_x$ (x = 0, 1, 2 at.%) alloy ribbons.

Table 1. Thermal parameters and the activation energies calculated using the Kissinger equation of the as-spun $Fe_{80.2}Si_3B_{12\text{-}x}P_2Nb_2Cu_{0.8}Ge_x$ (x = 0, 1, 2 at.%) alloy ribbons for the primary crystallization reaction.

Sample	T_c (K)	T_{x1} (K)	T_{p1} (K)	E_{x1} (kJ/mol)	E_{p1} (kJ/mol)
Ge0	553	725.9	740.5	268.6	491.3
Ge1	557	710.3	725.5	252.2	459.7
Ge2	562	702.3	718.1	250.9	446.1

In order to extend the qualitative analysis to a basic quantitative understanding of the crystallization mechanism, the on-isothermal crystallization kinetics of the primary crystallization process, at a heating rate of 20 K/min for the alloys, is studied by the Bla'zquez method [28]. For a crystallization process, the crystallization volume fraction $\alpha(T)$ can be expressed by the following equation:

$$\alpha(T) = \frac{\int_{T_0}^{T}(dH/dT)}{\int_{T_\infty}^{T_0}(\mathrm{dH/dT})} = \frac{A_T}{A}, \quad (2)$$

where T_∞ is the end crystallization temperature; $\mathrm{d}H/\mathrm{d}T$ is the heat capacity at atmospheric pressure; A_T and A are the areas of crystallization peak in the isochronal DSC trace from T_0 and T to T_∞, respectively. The crystallization volume fraction $\alpha(T)$ at the heating rate of 20 K/min for the primary crystallization reaction of the alloys is plotted as shown in Figure 6. It can be seen that the $\alpha(T)$ plot of all the alloys shows a typical S-shaped response. The slope of the $\alpha(T)$ plot corresponds to the crystallization rate in the crystallization process. The S-shaped curve indicates that the crystallization of the alloys occurs through the nucleation and growth process, which can be roughly divided into three stages. The initial stage with $0 < \alpha < 0.03$, in which the slop of the $\alpha(T)$ plot is small, corresponds to the nucleation process. It can be seen that the holding time in the first stage gradually decreases as the Ge content increases for the present alloys. This may be a higher Ge content results in more pre-existing nuclei in the alloy ribbons, which reduces nucleation activation energy, and thus shortens the nucleation time. The middle stage with $0.03 < \alpha < 0.9$, in which the $\alpha(T)$ plot is very steep, corresponds to the grain growth process. In this stage the crystal nucleus grows rapidly after nucleation, resulting in a sharp increase in the crystallization rate of the alloy. In the last stage with $0.9 < \alpha < 0.1$, the increase in crystallization rate slows down significantly, which is mainly because the amorphous matrix is exhausted, resulting in the limited growth space of grains.

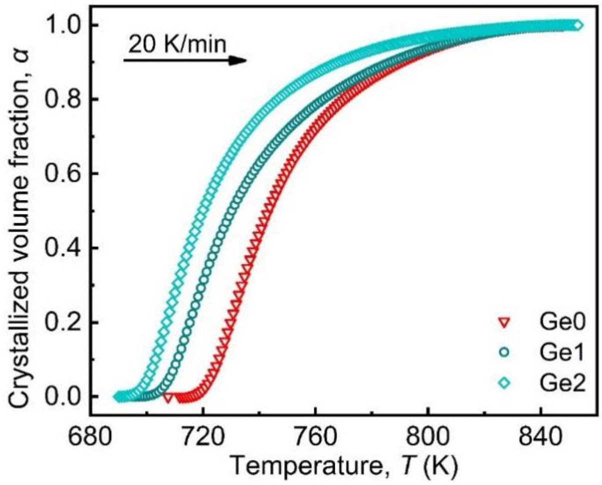

Figure 6. Curves of crystallization volume fraction versus temperature T for the first crystallization peak of the alloys ribbon at different heating rates.

Next, we analyzed the nucleation and growth mechanism for the first crystallization reaction of the alloys by calculating the local Avrami index n as the function of α based on the Johnson–Mehl–Avrami–Kolmogorov (JMAK) model. The crystallization kinetics of the alloys during isothermal heating can be expressed by the JMAK equation as [29]:

$$\alpha(t) = 1 - \exp\left[-k(t - t_0)^n\right], \tag{3}$$

where n is the Avrami index, t_0 is the induction time, and $k(T)$ is the kinetic coefficient as a function of temperature. Equation (3) can be written as [30]:

$$\ln[-\ln(1-\alpha)] = n[\ln k(T) + n\ln(t - t_0)]. \tag{4}$$

Under the approximation of the isokinetic behavior proposed by Nakamura et al., the relationship between α and temperature T and time t is:

$$\alpha = 1 - \exp\left\{-[\int_{t_0}^{t} k(T)dt]^n\right\}. \tag{5}$$

Further, the JMAK equation can be extended to non-isothermal kinetics under the isokinetic approximation [31]. For isochronous transformation, $\frac{dT}{dt}$ is equal to the heating rate β, and so Equation (5) can be written as:

$$\alpha = 1 - \exp\left\{-[\frac{1}{\beta}\int_{T_x}^{T} k(T)dT]^n\right\}, \tag{6}$$

where T_x is the onset temperature of the crystallization reaction. Blázquez et al. make a hypothesis of $\int_{T_x}^{T} k(T)dT = k\prime(T - T_x)$, and so Equation (6) can be rewritten as [28]:

$$\alpha = 1 - \exp\left\{-[k'(T - T_x)/\beta]^n\right\}, \tag{7}$$

where k' is a new frequency factor. Suppose that there is an Arrhenius dependency between k' and T, i.e., k' can be expressed as $k'(T) = k'_0\exp(-E/RT)$, where k'_0 is a constant and E is the activation energy. Therefore, the following equation can be obtained from Equation (7) [28,32,33].

$$n(\alpha) = \frac{1}{1 + E/RT(1 - T_x/T)} \frac{d\{\ln[-\ln(1-\alpha)]\}}{d\left\{\frac{\ln(T - T_x)}{\beta}\right\}} \tag{8}$$

The curve of ln $[-\ln(1-\alpha)]$ versus ln $[(T-T_0)/\beta]$ is shown in Figure 7a, and from this and Equation (8), the variation of the local Avrami index n with the crystallized volume fraction α can be plotted as shown in Figure 7b. The value of n involves information about the nucleation and growth mechanism of the crystallization process and is expressed as [33,34]:

$$n = a + bp \tag{9}$$

where a, b, and p are the nucleation index, growth dimension index, and growth index, respectively. Different values of a, b, and p reflect the different nucleation and growth mechanisms of the crystallization process [30,32]. It can see in Figure 7b that the value of the n of the first crystallization reaction of the Ge0, Ge1 and Ge2 alloys is essentially within the range of $n < 1$. The growth index, p, can be taken as 0.5 for Fe-based amorphous alloys [30]. Due to the small thickness of the alloy ribbon, the growth of nanocrystals along the thickness direction of the alloy ribbon may be restricted during the crystallization process, and thus the growth dimension index, b, should be less than 3. Based on the Equation (9), the nucleation index, a, for the present alloy ribbons can only be equal to 0, indicating the crystallization process of the direct growth of pre-existing nuclei. Therefore, it can be suggested that there are a large number of pre-existing nuclei in the α-Fe phase and precipitated Cu clusters in the as-spun alloy ribbons, which provide numerous heterogeneous nucleation sites to form dense and uniform α-Fe nanocrystals with a fine grain size.

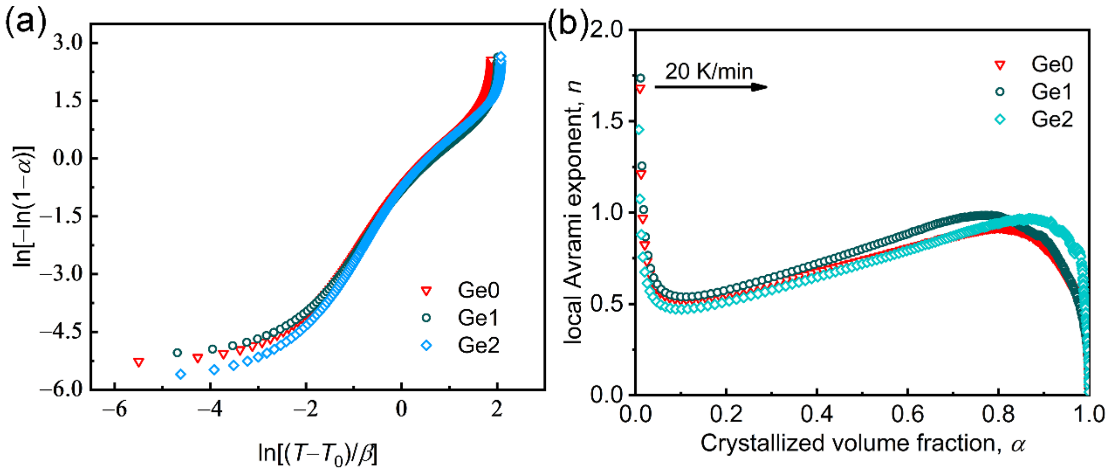

Figure 7. Plots of ln $[-\ln(1-\alpha)]$ versus ln$[(T-T_0)/\beta]$ (**a**) and local Avrami exponent, n, as a function of crystallized volume fraction α for the first crystallization peak of the alloys at a heating rate of 20 K/min (**b**).

4. Conclusions

In this work, $Fe_{80.2}Si_3B_{12-x}P_2Nb_2Cu_{0.8}Ge_x$ (x = 0, 1, 2 at.%) nanocrystalline alloys with excellent soft magnetic properties were prepared through the conventional heat treatment of the corresponding amorphous alloy ribbons, and the effects of Ge on magnetic properties and crystallization process of the alloys were thoroughly investigated. The results obtained are as follows:

- As the Ge content increases, the onset crystallization temperature of the first crystallization reaction (T_{x1}) and that of the second crystallization temperature (T_{x2}) of the as-spun $Fe_{80.2}Si_3B_{12\text{-}x}P_2Nb_2Cu_{0.8}Ge_x$ (x = 0, 1, 2 at.%) amorphous alloy ribbons shift to the low- and high-temperature directions, respectively, resulting in an increase in the heat treatment window ΔT (= $T_{x2} - T_{x1}$) from 149.9 K for x = 0 to 173.6 K for x = 2 in the Ge2. A larger ΔT is better for promoting the precipitation of α-Fe and inhibiting the precipitation of borides and phosphides, which is more conducive to the preparation of dense and uniform nanocrystals.

- The $Fe_{80.2}Si_3B_{10}P_2Nb_2Cu_{0.8}Ge_2$ nanocrystalline alloys with a small grain size of 15.7 nm were obtained by annealing the corresponding amorphous alloy ribbons at a temperature of 843 K for 10 min. The $Fe_{80.2}Si_3B_{10}P_2Nb_2Cu_{0.8}Ge_2$ nanocrystalline alloy exhibits excellent magnetic properties with a high B_s of 1.65 T, small H_c of 3 A/m, which are considered to be derived from uniform and dense nanocrystalline structures.
- Both the nucleation crystallization activation energy (E_{x1}) and the growth crystallization activation energy (E_{p1}) for the primary crystallization reaction of the as-spun Fe-based alloy ribbons decrease with increasing the Ge content.
- The non-isothermal crystallization kinetics study shows that the value of the local Avrami exponent, n, for the crystallization is less than 1 in the whole crystallization process, reflecting the crystallization mechanism of the direct growth of pre-existing nuclei.

Author Contributions: Conceptualization, Y.D. and Q.L.; methodology, H.Z.; software, H.Z.; validation, H.Z., F.B. and L.X.; formal analysis, A.H. and J.L.; investigation, H.Z.; resources, Y.D. and Q.L.; data curation, H.Z.; writing—original draft preparation, H.Z. and F.B.; writing—review and editing, Y.D. and Q.L.; supervision, Y.D. and Q.L.; project administration, Y.D. and Q.L.; funding acquisition, Y.D. and Q.L. All authors have read and agreed to the published version of the manuscript.

Funding: This work was supported by the National Key R&D Program of China (Grant No. 2021YFB3803000), Youth Innovation Promotion Association CAS (Grant No. 2021294), the National Natural Science Foundation of China (Grant No. 51801224), and the Tianshan Innovation Team Program of Xinjiang Uygur Autonomous Region (Grand No. 2020D14038).

Data Availability Statement: Data presented in this article are available at request from the corresponding author.

Conflicts of Interest: The authors declare no conflict of interest.

References

1. Herzer, G. Modern soft magnets: Amorphous and nanocrystalline materials. *Acta Mater.* **2013**, *61*, 718–734. [CrossRef]
2. Yoshizawa, Y.; Oguma, S.; Yamauchi, K. New Fe-based soft magnetic alloys composed of ultrafine grain structure. *J. Appl. Phys.* **1988**, *64*, 6044–6046. [CrossRef]
3. Suzuki, K.; Parsons, R.; Zang, B.; Onodera, K.; Kishimoto, H.; Kato, A. Copper-free nanocrystalline soft magnetic materials with high saturation magnetization comparable to that of Si steel. *Appl. Phys. Lett.* **2017**, *110*, 012407. [CrossRef]
4. Urata, A.; Matsumoto, H.; Yoshida, S.; Makino, A. Fe–B–P–Cu nanocrystalline soft magnetic alloys with high B_s. *J. Alloys Compd.* **2011**, *509*, S431–S433. [CrossRef]
5. Wang, S.; Jiang, W.; Hu, H.; Liu, P.; Wu, J.; Zhang, B. Roles of Co element in Fe-based bulk metallic glasses utilizing industrial FeB alloy as raw material. *Prog. Nat. Sci. Mater. Int.* **2017**, *27*, 503–506. [CrossRef]
6. Wang, F.; Inoue, A.; Han, Y.; Kong, F.L.; Zhu, S.L.; Shalaan, E.; Al-Marzouki, F.; Obaid, A. Excellent soft magnetic Fe-Co-B-based amorphous alloys with extremely high saturation magnetization above 1.85 T and low coercivity below 3 A/m. *J. Alloys Compd.* **2017**, *711*, 132–142. [CrossRef]
7. Liu, Q.; Liu, H.; Wang, M.; Zhang, Y.; Ma, Z.; Zhao, Y.; Yang, W. Effects of Ni substitution for Fe on magnetic properties of $Fe_{80-x}Ni_xP_{13}C_7$ (x= 0–30) glassy ribbons. *J. Non-Cryst. Solids* **2017**, *463*, 68–71. [CrossRef]
8. Liu, T.; He, A.; Kong, F.; Wang, A.; Dong, Y.; Zhang, H.; Wang, X.; Ni, H.; Yang, Y. Heterostructured crystallization mechanism and its effect on enlarging the processing window of Fe-based nanocrystalline alloys. *J. Mater. Sci. Technol.* **2021**, *68*, 53–60. [CrossRef]
9. Li, H.; Wang, A.; Liu, T.; Chen, P.; He, A.; Li, Q.; Luan, J.; Liu, C. Design of Fe-based nanocrystalline alloys with superior magnetization and manufacturability. *Mater. Today* **2021**, *42*, 49–56. [CrossRef]
10. Bai, F.; Dong, Y.; Xie, L.; Li, Q.; He, A.; Jia, X.; Li, J.; Wang, X. Effect of pre-existing nuclei on microstructure and magnetic properties of high B_s FINEMET-like nanocrystalline alloys. *J. Mater. Sci.* **2021**, *56*, 9254–9262. [CrossRef]
11. Liu, T.; Kong, F.; Xie, L.; Wang, A.; Chang, C.; Wang, X.; Liu, C. Fe (Co) SiBPCCu nanocrystalline alloys with high B_s above 1.83 T. *J. Magn. Magn. Mater.* **2017**, *441*, 174–179. [CrossRef]
12. Li, Y.; Jia, X.; Zhang, W.; Zhang, Y.; Xie, G.; Qiu, Z.; Luan, J.; Jiao, Z. Formation and crystallization behavior of Fe-based amorphous precursors with pre-existing α-Fe nanoparticles—Structure and magnetic properties of high-Cu-content Fe-Si-B-Cu-Nb nanocrystalline alloys. *J. Mater. Sci. Technol.* **2021**, *65*, 171–181. [CrossRef]
13. Ramasamy, P.; Stoica, M.; Bera, S.; Calin, M.; Eckert, J. Effect of replacing Nb with (Mo and Zr) on glass forming ability, magnetic and mechanical properties of FeCoBSiNb bulk metallic glass. *J. Alloys Compd.* **2017**, *707*, 78–81. [CrossRef]
14. Li, Y.; Jia, X.; Xu, Y.; Chang, C.; Xie, G.; Zhang, W. Soft magnetic Fe-Si-B-Cu nanocrystalline alloys with high Cu concentrations. *J. Alloys Compd.* **2017**, *722*, 859–863. [CrossRef]

15. Wang, C.; Li, J.; Zhang, X.; Wu, J.; He, A.; Dong, Y. Effect of P microalloying on magnetic properties and structure of FeSiBNbCu nanocrystalline alloy. *J. Mater. Sci. Mater. Electron.* **2021**, *32*, 4177–4184. [CrossRef]
16. Zhang, C.; Chi, Q.; Zhang, J.; Dong, Y.; He, A.; Zhang, X.; Geng, P.; Li, J.; Xiao, H.; Song, J.; et al. Correlation among the amorphous forming ability, viscosity, free-energy difference and interfacial tension in Fe–Si–B–P soft magnetic alloys. *J. Alloys Compd.* **2020**, *831*, 154784. [CrossRef]
17. Murugaiyan, P.; Mitra, A.; Patro, A.K.; Roy, R.K.; Churyukanova, M.; Kaloshkin, S.; Shuvaeva, E.; Panda, A.K. Role of P on amorphization, microstructure, thermo-physical and soft magnetic properties of Fe-rich FeB(P)SiNbCu melt-spun alloys. *J. Magn. Magn. Mater.* **2019**, *492*, 165723. [CrossRef]
18. Zhang, X.; Dong, Y.; He, A.; Xie, L.; Li, F.; Chang, L.; Xiao, H.; Li, H.; Wang, T. Improvement of SMPs in Fe-Si-B-P-C-Cu-Nb alloys via harmonizing P and B. *J. Magn. Magn. Mater.* **2020**, *506*, 166757. [CrossRef]
19. Zhao, T.; Yu, H.; Sun, C.; Chen, C.; Hao, J. Effects of the substitution of Si with P on the glass forming ability, crystallization behavior, and magnetic properties of FeCuNbSiBP atomized powder. *J. Magn. Magn. Mater.* **2022**, *550*, 169087. [CrossRef]
20. Cremaschi, V.; Sánchez, G.; Sirkin, H. Magnetic properties and structural evolution of FINEMET alloys with Ge addition. *Physica B* **2004**, *354*, 213–216. [CrossRef]
21. Chang, C.; Xiang, Z.; Zhao, C.; Wang, A.; Song, R.; Pan, D. Enlarging heat-treatment processing windows of Fe-Si-B-P-Cu-M nanocrystalline alloys by doping transition metal elements. *J. Alloys Compd.* **2021**, *860*, 158420. [CrossRef]
22. Wang, F.; Inoue, A.; Han, Y.; Zhu, S.L.; Kong, F.L.; Zanaeva, E.; Liu, G.D.; Shalaan, E.; Al-Marzouki, F.; Obaid, A. Soft magnetic Fe-Co-based amorphous alloys with extremely high saturation magnetization exceeding 1.9 T and low coercivity of 2 A/m. *J. Alloys Compd.* **2017**, *723*, 376–384. [CrossRef]
23. Xie, Z.; Wang, Z.; Han, Y. Effect of Ge addition on structure and soft magnetic properties of Si-rich Fe-based nanocrystalline alloys. *J. Alloys Compd.* **2016**, *672*, 332–335. [CrossRef]
24. Wang, Y.; Xu, K.; Li, Q. Comparative study of non-isothermal crystallization kinetics between $Fe_{80}P_{13}C_7$ bulk metallic glass and melt-spun glassy ribbon. *J. Alloys Compd.* **2012**, *540*, 6–15. [CrossRef]
25. Rezaei-Shahreza, P.; Seifoddini, A.; Hasani, S. Non-isothermal kinetic analysis of nano-crystallization process in $(Fe_{41}Co_7Cr_{15}Mo_{14}Y_2C_{15})_{94}B_6$ amorphous alloy. *Thermochim. Acta* **2017**, *652*, 119–125. [CrossRef]
26. Blaine, R.L.; Kissinger, H.E. Homer Kissinger and the Kissinger equation. *Thermochim. Acta* **2012**, *540*, 1–6. [CrossRef]
27. Pratap, A.; Lad, K.N.; Rao, T.L.S.; Majmudar, P.; Saxena, N.S. Kinetics of crystallization of amorphous $Cu_{50}Ti_{50}$ alloy. *J. Non-Cryst. Solids* **2004**, *345–346*, 178–181. [CrossRef]
28. Blazquez, J.; Conde, C.; Conde, A. Non-isothermal approach to isokinetic crystallization processes: Application to the nanocrystallization of HITPERM alloys. *Acta Mater.* **2005**, *53*, 2305–2311. [CrossRef]
29. Malek, J. The applicability of Johnson-Mehl-Avrami model in the thermal analysis of the crystallization kinetics of glasses. *Thermochim. Acta* **1995**, *267*, 61–73. [CrossRef]
30. Ramasamy, P.; Stoica, M.; Taghvaei, A.H.; Prashanth, K.G.; Ravi, K.; Eckert, J. Kinetic analysis of the non-isothermal crystallization process, magnetic and mechanical properties of FeCoBSiNb and FeCoBSiNbCu bulk metallic glasses. *J. Appl. Phys.* **2016**, *119*, 073908. [CrossRef]
31. Nakamura, K.; Katayama, K.; Amano, T. Some Aspects of Nonisothermal Crystallization of Polymers. II. Consideration of Isokinetic Condition. *J. Appl. Polym. Sci.* **1973**, *17*, 1031–1041. [CrossRef]
32. Paul, T.; Loganathan, A.; Agarwal, A.; Harimkar, S.P. Kinetics of isochronal crystallization in a Fe-based amorphous alloy. *J. Alloys Compd.* **2018**, *753*, 679–687. [CrossRef]
33. Peng, C.; Chen, Z.H.; Zhao, X.Y.; Zhang, A.L.; Zhang, L.K.; Chen, D. Crystallization kinetics of Zr60Cu25Fe5Al10 bulk metallic glass. *J. Non-Cryst. Solids* **2014**, *405*, 7–11. [CrossRef]
34. Ouyang, Y.; Wang, L.; Chen, H.; Cheng, X.; Zhong, X.; Feng, Y. The formation and crystallization of amorphous $Al_{65}Fe_{20}Zr_{15}$. *J. Non-Cryst. Solids* **2008**, *354*, 5555–5558. [CrossRef]